A COUPLED ETAS-I²GMM POINT PROCESS WITH APPLICATIONS TO SEISMIC FAULT DETECTION[1]

BY YICHENG CHENG, MURAT DUNDAR AND GEORGE MOHLER

Indiana University–Purdue University Indianapolis

Epidemic-type aftershock sequence (ETAS) point process is a common model for the occurrence of earthquake events. The ETAS model consists of a stationary background Poisson process modeling spontaneous earthquakes and a triggering kernel representing the space–time-magnitude distribution of aftershocks. Popular nonparametric methods for estimation of the background intensity include histograms and kernel density estimators. While these methods are able to capture local spatial heterogeneity in the intensity of spontaneous events, they do not capture well patterns resulting from fault line structure over larger spatial scales. Here we propose a two-layer infinite Gaussian mixture model for clustering of earthquake events into fault-like groups over intermediate spatial scales. We introduce a Monte Carlo expectation-maximization (EM) algorithm for joint inference of the ETAS-I²GMM model and then apply the model to the Southern California Earthquake Catalog. We illustrate the advantages of the ETAS-I²GMM model in terms of both goodness of fit of the intensity and recovery of fault line clusters in the Community Fault Model 3.0 from earthquake occurrence data.

1. Introduction.

1.1. *Background on point-process models of seismicity.* The epidemic-type aftershock sequence (ETAS) model of earthquake occurrence [Ogata (1988, 1998)] is a self-exciting point-process model where the conditional intensity $\lambda(t, x, y|H_t)$ of events is determined by a stationary Poisson intensity generating spontaneous earthquake events along with a dynamic term representing a branching process of aftershocks:

$$(1) \qquad \lambda(t, x, y|H_t) = \mu(x, y) + \sum_{i:t_i<t} g(t - t_i, x - x_i, y - y_i, m_i).$$

Here (x, y) is the epicenter of an earthquake event described by longitude and latitude in decimal degrees, m is its magnitude on the Richter scale computed using a body-wave magnitude formula [Spence, Sipkin and Choy (1989)], $H_t = \{(t_i, x_i, y_i, m_i) : t_i < t\}$ is the history of all earthquake events up to time t in a

catalog, and $\mu(x, y)$ is the background intensity reflecting spatial heterogeneity of spontaneous earthquakes and the fact that earthquake catalogs with aftershocks removed are approximately Poisson in time [Gardner and Knopoff (1974)].

The space–time-magnitude distribution of parent-offspring events in the branching process given by the function $g(t, x, y, m)$ is called the triggering kernel, typically following Omori's law [Utsu (1961)]:

$$g(t - t_i, x - x_i, y - y_i, m_i)$$

$$(2) \qquad = \frac{K_0 e^{a(m_i - m_0)}}{(t - t_i + c)^{(1+\omega)}((x - x_i)^2 + (y - y_i)^2 + d)^{(1+\rho)}},$$

where m_0 is the cutoff magnitude of the dataset under study [Ogata (1988)] and $(K_0, a, c, \omega, d, \rho) > 0$ are parameters to be estimated. Estimation of equation (1) typically consists of constructing a nonparametric estimate for $\mu(x, y)$ along with finding maximum-likelihood estimators for the parameters of the triggering kernel in equation (2). Methods for maximizing the likelihood include quasi-Newton [Ogata (1988)] and expectation-maximization (EM) [Veen and Schoenberg (2008)], and the most common estimators for $\mu(x, y)$ are spatial histograms [Marsan and Lengline (2008), Veen and Schoenberg (2008)] or isotropic kernel density estimators [Adelfio and Chiodi (2015), Zhuang, Ogata and Vere-Jones (2002)].

1.2. *A new model*: *Coupled ETAS-I²GMM.* Earthquakes cluster at multiple scales, as earthquakes cluster locally through aftershock activity but also over larger scales along fault lines (see Figure 1). While there is research on the reconstruction of aftershock clusters from event data [Zaliapin et al. (2008), Zhuang, Ogata and Vere-Jones (2002)], existing point-process models of earthquake activity fail to capture spatial clustering patterns at the larger scale of fault lines. In particular, histograms and kernel density estimators are able to capture spatial heterogeneity in the risk of spontaneous earthquakes, but the methods capture variation over only one scale. To our knowledge, our work here is the first to attempt to reconstruct the community fault model [Plesch et al. (2007)] with a statistical model based on earthquake event data.

In this paper we introduce a new type of ETAS model that can capture multiscale clustering in earthquake patterns. In particular, we propose using an infinite mixture of infinite Gaussian mixtures (I²GMM) [Yerebakan, Rajwa and Dundar (2014)] to estimate the background rate of earthquakes $\mu(x, y)$. For each spatial cluster, the I²GMM uses a different Dirichlet process mixture of Gaussians (DPMG) that simultaneously predicts the number of clusters along with performing model inference. While I²GMM has been introduced for high-dimensional clustering and ETAS is well known in seismology, what is new in this paper is the use of I²GMM for modeling the intensity of a point process and the coupling of these two techniques for multiscale modeling of space–time event patterns. Through the use of an expectation-maximization algorithm, the benefit of
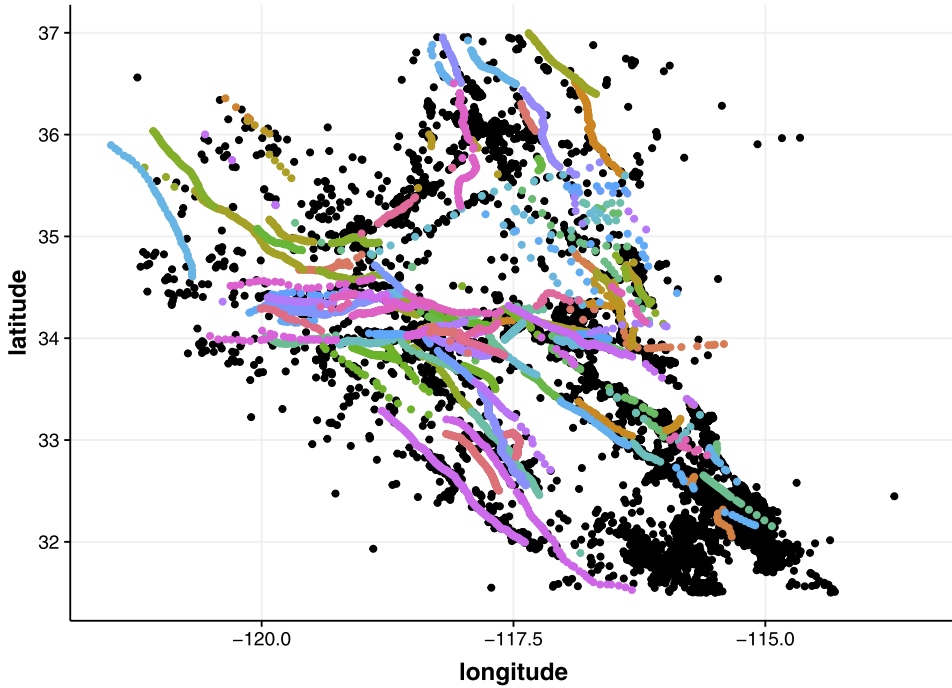
FIG. 1. *Southern California earthquakes magnitude* 2.5 *and greater* (*black*) *and faults corresponding to the Community Fault Model* 3.0 (*marked by lines*).

our approach is that earthquakes are assigned membership to aftershock clusters in addition to a larger scale fault line cluster.

Another advantage of our approach is that multi-modal and skewed spatial clusters are more accurately captured. In the case of spatial earthquake patterns, each fault may be considered as a separate cluster with multi-modality and skewness that the I^{2}GMM can handle better than histograms and KDE estimators. In particular, a fault is represented in the background rate of spontaneous earthquakes by I^{2}GMM as a cluster of several Gaussians. Unlike kernel density estimation where each kernel corresponds to one event in the dataset at which it is centered, each Gaussian in a spatial cluster of I^{2}GMM is not necessarily centered at a historical event and can generate multiple spontaneous earthquakes in the future. One additional advantage of the I^{2}GMM model is that earthquakes are assigned membership to spatial clusters inferred by the model. In this research, we explore the relevance of spatial cluster membership to automatic detection of fault lines within the ETAS-I^{2}GMM framework.

1.3. *Outline of the paper.* In Section 2 we describe our methodology, including an overview of the I^{2}GMM model and details on a Monte Carlo EM algorithm for joint inference of the ETAS-I^{2}GMM model. In Section 3 we present results for

several experiments where the ETAS-I^{2}GMM is applied to a Southern California earthquake catalog [SCEDC (2013)]. We compare the goodness of fit of the estimated intensity of the model to a baseline approach. We also use the Community Fault Model 3.0 [Plesch et al. (2007)] to explore the ability of the ETAS-I^{2}GMM model to detect fault locations and event-fault linkage from space–time event data.

2. Methods.

2.1. *Infinite mixture of infinite Gaussian mixtures.* The finite Gaussian mixture model (GMM) uses a single Gaussian for each cluster and requires the number of clusters to be specified. In the infinite version of GMM (IGMM) [Ferguson (1973)], the number of components is estimated along with the component mean vectors and covariances. Both GMM and IGMM are used for clustering problems, albeit with limited success, as these techniques often overestimate the number of mixture components so as to more accurately estimate the density of the underlying dataset. However, a more accurate estimation of the density does not necessarily translate into a more accurate estimation of cluster distributions, as density estimation does not readily solve the problem of many-to-one mappings between components and clusters. Two different approaches to overcome this limitation are considered in the literature.

The first approach replaces Gaussian mixture components by Student-t [Andrews and McNicholas (2012), Archambeau and Verleysen (2007), Peel and McLachlan (2000), Svensén and Bishop (2005)] or skewed-t [Lee and McLachlan (2014)] distributions and their Pearson-type extensions [Forbes and Wraith (2014), Sun, Kaban and Garibaldi (2010)] in an effort to better model cluster distributions with heavy tails. Although closed-form solutions for maximum-likelihood estimations of parameters do not in general exist under these settings, extensions of the EM algorithm can still be derived for this family of mixture models by placing certain restrictions on the original model. This line of models has proved quite effective in clustering datasets with skewed distributions but are less ideal for clusters with multi-mode distributions.

The second approach generates a large number of Gaussian components and merges them according to various metrics in an effort to recover true cluster distributions. The study in [Figueiredo and Jain (2002)] initializes the model with a large number of components and uses the concept of minimum message length to merge components. Another technique uses the Bayesian information criterion (BIC) to choose the initial number of components and merges components to minimize entropy [Baudry et al. (2010)]. Other options for assigning components to clusters include clustering modes of components [Ge and Sealfon (2012)] and ridgeline analysis and Bhattacharyya dissimilarity [Hennig (2010)]. Compared to mixtures of Student-t or skewed-t distributions, this line of models is more flexible in terms of the type of distributions they can model. However, the main limitation of these techniques is the independence assumption made during component estimation

that makes EM derivations possible. These techniques assume that all components are generated independently, which is not a very realistic assumption in a setting where some clusters are known to be multi-mode, and components originating from the same cluster are more likely to share certain latent parameters than do two random components. Another limitation of these techniques is the computational complexity that increases with the square of the number of Gaussian components, as the decision to merge two components requires evaluating the metric for every possible pair of components. This puts a constraint on the maximum number of components that can be used to model datasets.

When clustering datasets with skewed/multi-mode cluster distributions, two dependent subproblems, namely density estimation and component clustering, need to be addressed jointly. The two-layer nonparametric GMM (I^2GMM) model, which can grow arbitrarily large in the number of components and clusters generated, was introduced earlier to more accurately cluster datasets with multi-mode and skewed cluster distributions [Yerebakan, Rajwa and Dundar (2014)].

In I^2GMM the lower layer estimates the density of the overall dataset by clustering individual data points to components, while the upper layer associates components with clusters to allow for cluster recovery. In the ETAS-I^2GMM model, each upper layer cluster of I^2GMM corresponds to a fault in the background rate and events assigned to an upper-layer cluster are assumed to be spontaneously triggered by that fault. We note that upper-layer cluster membership is separate from space–time aftershock clustering generated by the triggering kernel, though aftershock clustering may be used to link offspring events back to a fault line. The lower-layer clusters of I^2GMM serve to represent complicated geometries within a single fault (for example, a fault that is not straight but instead bends) and represent different families of background events within a single fault that could be viewed as sub-faults. The generative model of I^2GMM is a two-layer hierarchical Dirichlet process mixture (DPM) model where the lower layer uses one DPM for each cluster and the upper layer uses a global DPM for modeling cluster shapes and sizes. The dependency between the two layers is achieved by centering the base distributions of DPMs in the lower layer on a unique parameter distributed according to the global DPM. Inference, which involves sampling component indicator variables for individual data points and sampling cluster indicator variables for components, is performed by a collapsed Gibbs sampler, enabling optimization of two subproblems simultaneously.

We believe that I^2GMM has three unique features that make it very suitable for the estimation of background intensity $\mu(x, y)$ in the ETAS model.

- As a two-layer nonparametric model, I^2GMM allows the number of clusters and the number of mixture components in each cluster to grow arbitrarily large, offering great flexibility in modeling clusters with multi-mode/skewed distributions. This is the main feature that distinguishes I^2GMM from other model-based clustering techniques that use one component for each cluster.

- As a Bayesian model, I^{2}GMM has hyper-parameters that can be tuned to recover clusters with varying shapes and different levels of rarity without facing singularities during model estimation. This distinguishes I^{2}GMM from purely data-driven techniques such as finite mixture of Gaussians and t-distributions that rely on EM and its extensions during model learning.
- As a hierarchical model, I^{2}GMM can share parameters not only across different clusters but also across different components of the same cluster. In other words, I^{2}GMM assumes that components are generated independently only when conditioned on the unique parameter defining their clusters of origin. This differentiates the proposed work from other techniques that estimate a large number of Gaussian components and merges them sequentially to recover clusters, thus violating component dependence.

In Figure 2 we provide an illustration of the generative model for I^{2}GMM: t_{kl} indicates the lth component in the kth cluster C_k; x_{kl_i} indicates the ith data point in the lth component in the kth cluster. In the generative process, t_{kl} is a Gaussian distribution and C_k is a Gaussian mixture defined by its components. We will

Clusters C_k

With means and covariances (μ_k, Σ_k) generated by a Dirichlet process of base distribution $H = (\mu|\mu_0, \Sigma\kappa_0^{-1})W^{-1}(\Sigma|\Psi_0, m)$

Position of μ_k is marked by asterisk while the oval illustrates its covariance matrix.

Components t_{kl}

With mean μ_{kl} generated by a second layer Dirichlet process of base distribution $H_k = N(\mu_k, \Sigma_k\kappa_1^{-1})$, and covariance Σ_k of its cluster.

Position of μ_{kl} is marked by x while the dashed oval illustrates its covariance matrix.

Data points x_{kli}

Generated by $x_{kli} \sim N(\mu_{kl}, \Sigma_k)$

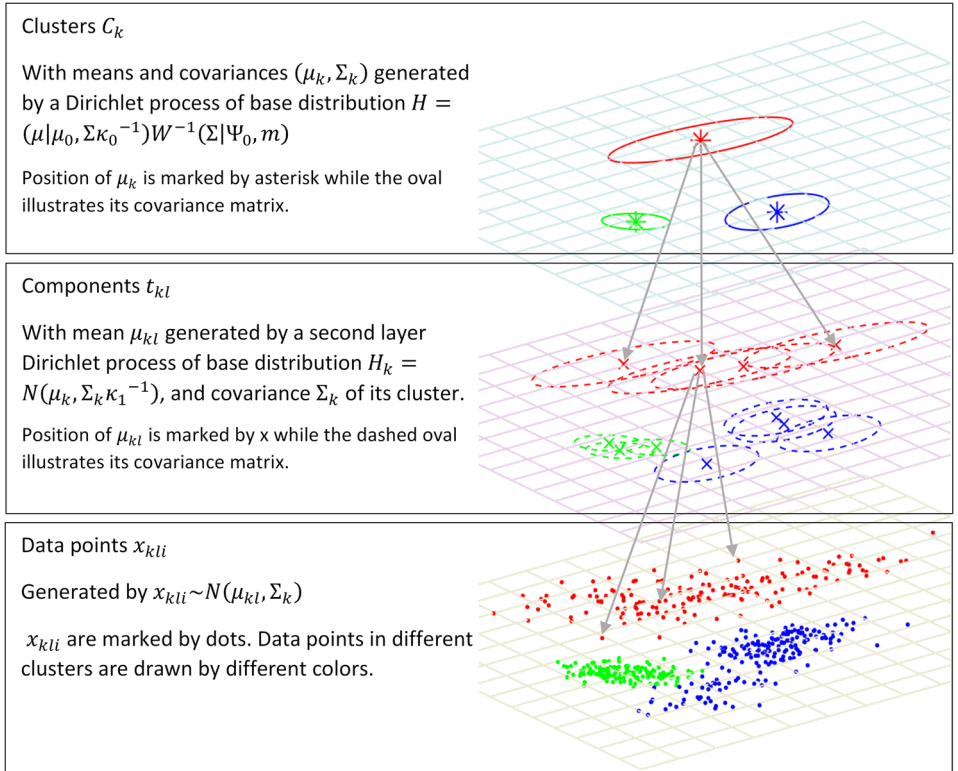x_{kli} are marked by dots. Data points in different clusters are drawn by different colors.

FIG. 2. *The hierarchy of I^{2}GMM model illustrated on a synthetic dataset.*

use the top-level label (i.e., C_k) to identify different clusters of spontaneous earthquakes that can be used to predict fault membership of each event. The lower-level labels could also be used to identify faults or sub-faults (where seismologists may want to consider refining their labels); however, in this paper we will restrict our analysis to the top-level labels.

The generative model for I^{2}GMM is given by

$$H = \text{NIW}(\mu, \Sigma | \mu_0, \Psi_0, \kappa_0, m) = N(\mu | \mu_0, \Sigma \kappa_0^{-1}) W^{-1}(\Sigma | \Psi_0, m),$$

$$G \sim \text{DP}(\gamma H),$$

$$(\mu_k, \Sigma_k) = \theta_k \sim G,$$

$$(3) \qquad H_k = N(\mu_k, \kappa_1^{-1} \Sigma_k),$$

$$G_k = \text{DP}(\alpha H_k),$$

$$\mu_{kl} \sim G_k,$$

$$x_{kl_i} \sim N(\mu_{kl}, \Sigma_k).$$

In this generative model $\text{DP}(\gamma H)$ is a global Dirichlet process with normal-inverse-Wishart base distribution H and a concentration parameter γ. G is a discrete mixing measure sampled from the global DP. Center μ_k and covariance Σ_k of the cluster k are drawn from G. For each cluster generated by the global DPM, a local DPM is defined with base distribution H_k and concentration parameter α. All H_k are Gaussian distributions with centers μ_k and covariances $\kappa_1^{-1} \Sigma_k$. G_k is the cluster-specific discrete mixing measure drawn from the local DP. The components in cluster k are generated with mean vectors μ_{kl} drawn from G_k. Data points x_{kl_i} are generated from the Gaussian components with mean vectors μ_{kl} and covariance matrices Σ_k. User-specified hyper-parameters $(\mu_0, \Psi_0, \kappa_0, \kappa_1, \alpha, \gamma, m)$ are listed in Table 1 along with their descriptions.

To perform inference with the I^{2}GMM model using spatial event data, we first initialize the cluster and component indicators for each event to some arbitrary values (for example, put all data in the same component of a cluster) and then use a collapsed Gibbs sampler to infer values for indicator variables one at a time, given all other indicator variables [Yerebakan, Rajwa and Dundar (2014)]. Conditioned on the indicator variables, the location vectors and scale matrices are determined by maximizing the complete data log-likelihood and have closed-form solutions. One sweep of the Gibbs sampler will go over all events in the dataset; convergence typically requires several hundred to thousand Gibbs sweeps.

2.2. *EM inference for ETAS.* The ETAS model given in equation (1) can be viewed as a branching process where spontaneous events occur according to a Poisson process with intensity $\mu(x, y)$. Events (from all generations) give birth to direct offspring events determined by the triggering kernel $g(t - t_i, x - x_i, y - y_i, m_i)$.

TABLE 1
Hyper-parameters for I^2GMM

μ_0	Expected mean vector for each cluster. This is usually set to the mean of the overall dataset.
Ψ_0	$\frac{\Psi_0}{m-d-1}$ is the expected covariance matrix for clusters. This is usually set to identity.
κ_0	A positive scaling constant that adjusts the separation among clusters. The smaller the κ_0, the more separated the clusters will be from each other.
κ_1	A positive scaling constant that adjusts the separation among components of a given cluster. The smaller the κ_1, the more separated the components will be from each other, and clusters will tend to emerge with multi-modal distributions.
α	The concentration parameter for the local DPMs that controls the expected number of components and their sizes within a cluster.
γ	The concentration parameters for the global DPM that controls the expected number of clusters and their sizes.
m	Degree of freedom for the inverse Wishart that controls the degree of deviation of actual component covariances from the expected covariance. The higher the m, the less the deviation and the more similar component shapes will be.

Given an initial guess for the parameters of the triggering kernel in equation (2) and the background rate $\mu(x, y)$, the branching structure along with the model parameters of the triggering kernel can be estimated using an EM algorithm [Mohler et al. (2011), Veen and Schoenberg (2008)]. In the E-step of the EM algorithm the probability p_{ij} that event i is a direct offspring of event j is estimated, along with the probability p_i^b that the event was generated by the Poisson process with rate $\mu(x_i, y_i)$:

$$(4) \qquad p_{ij} = \frac{g(t_i - t_j, x_i - x_j, y_i - y_j)}{\lambda(t_i, x_i, y_i)},$$

$$(5) \qquad p_i^b = \frac{\mu(x_i, y_i)}{\lambda(t_i, x_i, y_i)}.$$

Given the probabilistic estimate of the branching structure, the complete data log-likelihood is then maximized in the M-step (using standard methods for estimating a Pareto distribution) [Veen and Schoenberg (2008)], providing an estimate of the model parameters.

2.3. *Joint inference of the ETAS-I^2GMM.* We propose three variants for inferring the joint ETAS-I^2GMM model.

ETAS-I^2GMM 1. In the first variant we start by clustering all events spatially using I^2GMM. We then evaluate the convex hull of each cluster and enforce $\mu(x, y)$ to be constant in the convex hull. $\mu(x, y)$ and other parameters are then estimated using the EM algorithm in Section 2.2 with the rectangular cells in Section 2.4 replaced by the estimated convex hulls.

ETAS-I^2GMM 2. In the next variant we perform joint inference using a Monte Carlo EM algorithm. In particular, at each EM iteration we perform the following steps:

i. (I^2GMM-step) Sample background events from probabilistic branching structure p_{ij}. Rather than clustering all events using I^2GMM now we cluster the sampled background events only. Estimate $\mu(x, y)$ based on the clusters of background events the same as in ETAS-I^2GMM 1.

ii. (E-step) Estimate probabilistic branching structure and model parameters of triggering kernel as in Section 2.2.

ETAS-I^2GMM 3. In the last variant we use a weighted I^2GMM algorithm in place of the i step in variant two above. Instead of estimating $\mu(x, y)$ based on clusters of sampled background events, we estimate $\mu(x, y)$ based on clusters generated by weighted I^2GMM on all events whose weights are estimated by (5). In the first EM iteration, since p_i^b does not exist we initialize the weight to 1.

2.4. *Baseline ETAS model with histogram estimator.* We use the histogram estimator proposed in Veen and Schoenberg (2008) as a baseline model for comparison. In particular, we let the background rate $\mu(x, y)$ be a constant:

$$(6) \qquad \mu(x, y) = \mu_k \qquad \text{if } (x, y) \text{ is in cell } k, k \in 1, \ldots, K$$

over each rectangular cell of a regular grid. There are then $K + 6$ parameters $\theta = (\mu_1, \ldots, \mu_K, a, c, d, w, \rho, K_0)$ that we need to estimate (assuming there are K cells in the grid) and for that purpose we use the EM algorithm in Veen and Schoenberg (2008).

2.5. *ETAS model with variable kernel estimates.* For a second comparison we use kernel density estimation with variable bandwidth as proposed in Zhuang, Ogata and Vere-Jones (2002). Here $\mu(x, y)$ is estimated as

$$(7) \qquad \mu(x, y) = \frac{1}{T} \sum_j p_j^b k_{d_j}(x - x_j, y - y_j),$$

where T is the time span of all events, p_j^b is the background probability defined in (5), d_j is the varying bandwidth calculated for each event j according to the distance of its n_p nearest neighbor, and $k_d(x, y)$ denotes the Gaussian kernel function $\frac{1}{2\pi d} \exp\{-\frac{x^2+y^2}{2d^2}\}$. For all experiments, we set the parameter $n_p = 3$ as suggested by Zhuang (2011). The rest of the parameters are estimated according to Section 2.2 using the same EM algorithm.

3. Experiments and results.

3.1. *Experiment* 1: *Goodness of fit of ETAS-I^2GMM applied to CA earthquakes* 3.5 *and greater since* 2000.   We apply our models to the California earthquake-event data filtered by year (greater than 2000) and magnitude (greater than 3.5). The geographic bounds range from $46.116 >$ latitude > 29.615 and $-113.581 >$ longitude > -130.427. The dataset is divided into training and testing using time point 2010-01-01 00:00:00 as cutoff. All events before this time stamp are placed in the training dataset, while all events after it are placed in the testing dataset. We performed experiments with the following seven models to analyze how the performance varies by adopting different modeling strategies:

1. ETAS-I^2GMM 1.
2. ETAS-I^2GMM 2.
3. ETAS-I^2GMM 3.
4. 4×4 grid baseline model.
5. 3×4 grid baseline model.
6. 3×3 grid baseline model.
7. ETAS-KDE described in Section 2.5.

Note that experiments 1 to 3 are repeated 10 times and the means of the likelihoods are recorded. For I^2GMM we run 400 Gibbs sweeps; the hyper-parameters are set as follows: $\mu_0 = [36.4603; -119.3265]$ the mean of the dataset; $\Sigma_0 = [21.4972 \quad 0; 0 \quad 23.1351)]$ the diagonal matrix with diagonal entries equal to the latitude-longitude variances of the dataset; $m = 22$; $\kappa_0 = 0.1$; $\kappa_1 = 0.5$. The values of m, κ_0, κ_1 are tuned to let I^2GMM generate fewer or equivalent number of clusters as the 4×4 grid baseline model.

We use the log-likelihood function

$$(8) \qquad \mathrm{logL} = \sum_{i=1}^{N} \log\big(\lambda(t_i, x_i, y_i)\big) - \int_0^T \int_S \lambda(t, x, y)\, dx\, dy\, dt$$

to evaluate the competing models for the background intensity. The results are shown in Table 2.

All three ETAS-I^2GMM models outperform those with histogram or kernel density estimators. Between the three ETAS-I^2GMM variants, the best-performing model is variant 1, where I^2GMM is first estimated and the EM algorithm is run separately to estimate the parameters of the triggering kernel. It is worthwhile to note that finer clusters do not necessarily yield better results. Even though the 4×4 grid model generates more clusters it produces lower likelihood than the 3×4 grid model.

TABLE 2
Log-likelihood model comparison

Model	logL	$\sum_i \log(\lambda_i)$	$\int \lambda$
ETAS-I^{2}GMM 1	**−4619**	−1206	3413
ETAS-I^{2}GMM 2	−4686	−1283	3403
ETAS−I^{2}GMM 3	−4716	−1319	3397
4 × 4 Grid	−4980	−1590	3390
3 × 4 Grid	−4937	−1607	3330
3 × 3 Grid	−5023	−1582	3440
ETAS−KDE	−4860	−1441	3419

3.2. *Experiment* 2: *ETAS-I^{2}GMM for event-fault linkage from space–time event data.* Next, we investigate the extent to which the ETAS-I^{2}GMM model can learn fault structure from space–time event data. For this purpose we use the Community Fault Model 3.0 [Plesch et al. (2007)], which is a three dimensional representation (latitude, longitude, and elevation) of faults in Southern California. The CFM is a collaborative project undertaken by scientists of the Southern California Earthquake Center (SCEC) for studying active faults and earthquake phenomena and to improve regional earthquake hazard assessments. Our goal here is to assess how well ETAS-I^{2}GMM recovers a 2D projection of the CFM 3.0 using only space–time-magnitude earthquake incident data as input. In particular, we generate a fault label for each event in the dataset by assigning fault membership as the nearest fault in CFM 3.0 (see Figure 3).

The ETAS-I^{2}GMM-predicted label is taken from the first layer of the I^{2}GMM model clusters, where offspring events are assigned to the spatial cluster of their nearest neighbor among background events. To allow for comparison to the CFM 3.0, we restrict the geographic bounds of the CA earthquake event data to $36.958 >$ latitude > 31.518 and $-113.719 >$ longitude > -121.176, but we expand the magnitude threshold down to 2.5.

There are 145 actual fault lines in CFM 3.0, but all the models we used in previous experiments generate at most 26 clusters. For this dataset, we added two additional models in the experiments for fault recovery:

- An I^{2}GMM with parameters tuned to generate approximately 145 clusters on average; this version is named as ETAS-I^{2}GMM 145 in our experiments.
- A 16 × 15 grid model that contains 143 nonempty clusters.

Given that the number of clusters estimated by I^{2}GMM may be different from the number of faults in the CFM 3.0, we evaluate the success of fault-cluster recovery by considering the percentage of correctly classified data points. In addition to the overall clustering accuracy, we evaluate the mean clustering accuracy for the 10 largest faults, which contains 67% of data points across 145 faults. In Table 3
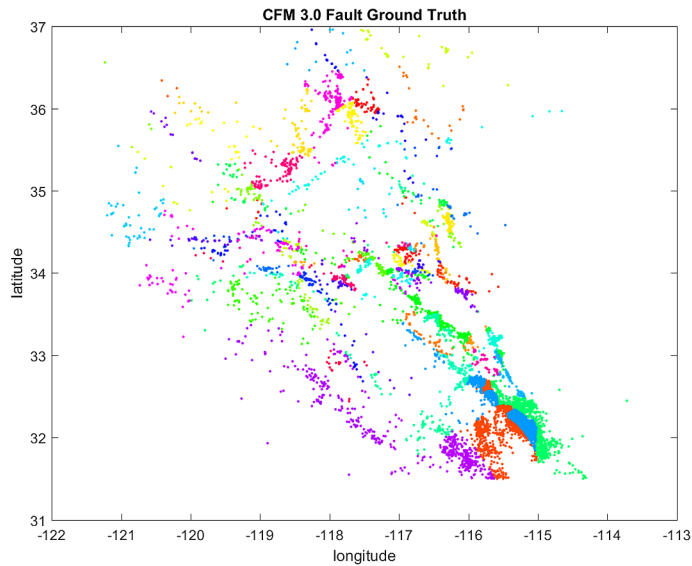
FIG. 3.   *Fault line cluster membership using the nearest CFM* 3.0 *fault to each earthquake* (*ground truth*).

we present the clustering accuracy for the seven models listed in 3.1 as well as the two additional models. To calculate the clustering accuracy, we first align the generated clusters with the ground-truth classes using the Hungarian algorithm [Kuhn (1955), Stephens (2000)], and then calculate the percentage of the data points that fall into their classes of origin. We adopt clustering accuracy for its simplicity and its invariance to potential misalignment between ground truth and predicted class

TABLE 3
Clustering accuracy comparison of fault classification. The log-likelihoods are also included. We are not able to evaluate the accuracy score for ETAS-KDE since it doesn't generate spatial clusters

	Accuracy	$\overline{Acc}_{10}$	logL	$\sum_i \log(\lambda_i)$	$\int \lambda$
ETAS-I2GMM 145	0.46	0.52	**5495**	16,772	11,277
ETAS-I2GMM 1	**0.50**	**0.67**	4688	16,034	11,346
ETAS-I2GMM 2	0.45	0.46	4466	15,820	11,354
ETAS-I2GMM 3	0.41	0.33	4495	15,904	11,409
Grid 16x15	0.45	0.47	4384	15,703	11,319
Grid 4x4	0.37	0.37	4247	15,723	11,476
Grid 3x4	0.36	0.28	4224	15,694	11,470
Grid 3x3	0.35	0.32	4198	15,673	11,475
ETAS-KDE	–	–	4066	15,464	11,398

labels. Mean clustering accuracy is calculated as below:

$$\overline{Acc} = \frac{1}{|C^*|} \sum_{C_k^* \in C^*} \frac{|C_k^* \cap C_k|}{|C_k^*|},$$

(9)

where for each event, C_k^* is fault cluster assignment of event k and C_k is the predicted cluster assignment of event k. Here C^* contains all fault clusters under consideration; C_k is the predicted cluster corresponding to C_k^* after alignment; $C_k^* \cap C_k$ indicates data points in both C_k^* and C_k; $|S|$ denote the cardinality of the set S. To compute the mean clustering accuracy for the 10 largest faults $\overline{Acc}_{10}$ we set C^* to contain the 10 largest true fault clusters in the above equation.

Here again we see that ETAS-I^{2}GMM 1 performs best both in terms of clustering accuracy and $\overline{Acc}_{10}$. All the ETAS-I2GMM models outperform ETAS with a histogram estimator or a kernel density estimator in terms of likelihood, which is consistent with the results we have in Experiment 1 on the CA earthquake data. In Figure 4 we plot the clusters recovered corresponding to ETAS-I^{2}GMM 145, ETAS-I^{2}GMM 1, 16×15 grid, 4×4 grid, and the true clusters for a better understanding of this outcome. Despite the fact that I^{2}GMM generated only 26 unique clusters on average compared to 145 actual fault lines in CFM 3.0, a meaningful clustering accuracy of 0.5 was achieved. Results suggest that a majority of events in fault clusters that tend to have elongated, skewed, and in some cases multi-mode shapes are clustered correctly by I^{2}GMM. In contrast, the clusters in the two histogram models have abrupt boundaries formed from the grid irrespective of the shape of the underlying faults, as shown in Figure 4. Moreover, when we adjust the parameters of the I^{2}GMM to get approximately the same number of clusters as the true number of fault clusters, we observe that the clustering accuracy does not improve owing to erroneous splitting of events belonging to larger fault lines into multiple clusters. This is also true for the 16×15 grid model that generates 143 nonempty clusters. Although the clustering accuracy improves with this model compared to the grid model with a smaller number of clusters, overall clustering accuracy achieved by this model is still less than that achieved by I^{2}GMM with 26 clusters (0.45 vs 0.50). The difference in clustering accuracy between the two models increases in favor of I^{2}GMM when we take into account only the largest 10 fault clusters (0.47 vs 0.67). This is a natural result of the grid model's arbitrarily splitting fault clusters, compared to the more effective handling of elongated fault cluster shapes by I^{2}GMM.

We illustrate this over-splitting problem in Figure 5 by plotting the clustering results of the 10 largest faults. From the $\overline{Acc}_{10}$ results in Table 3 and Figure 5 we can see that ETAS-I^{2}GMM 1 did the best by achieving a mean clustering accuracy of 0.67 across 10 faults while recovering several of them by a clustering accuracy of over 0.9. On the other hand, for the grid models the $\overline{Acc}_{10}$ values are consistent with their corresponding overall accuracies.
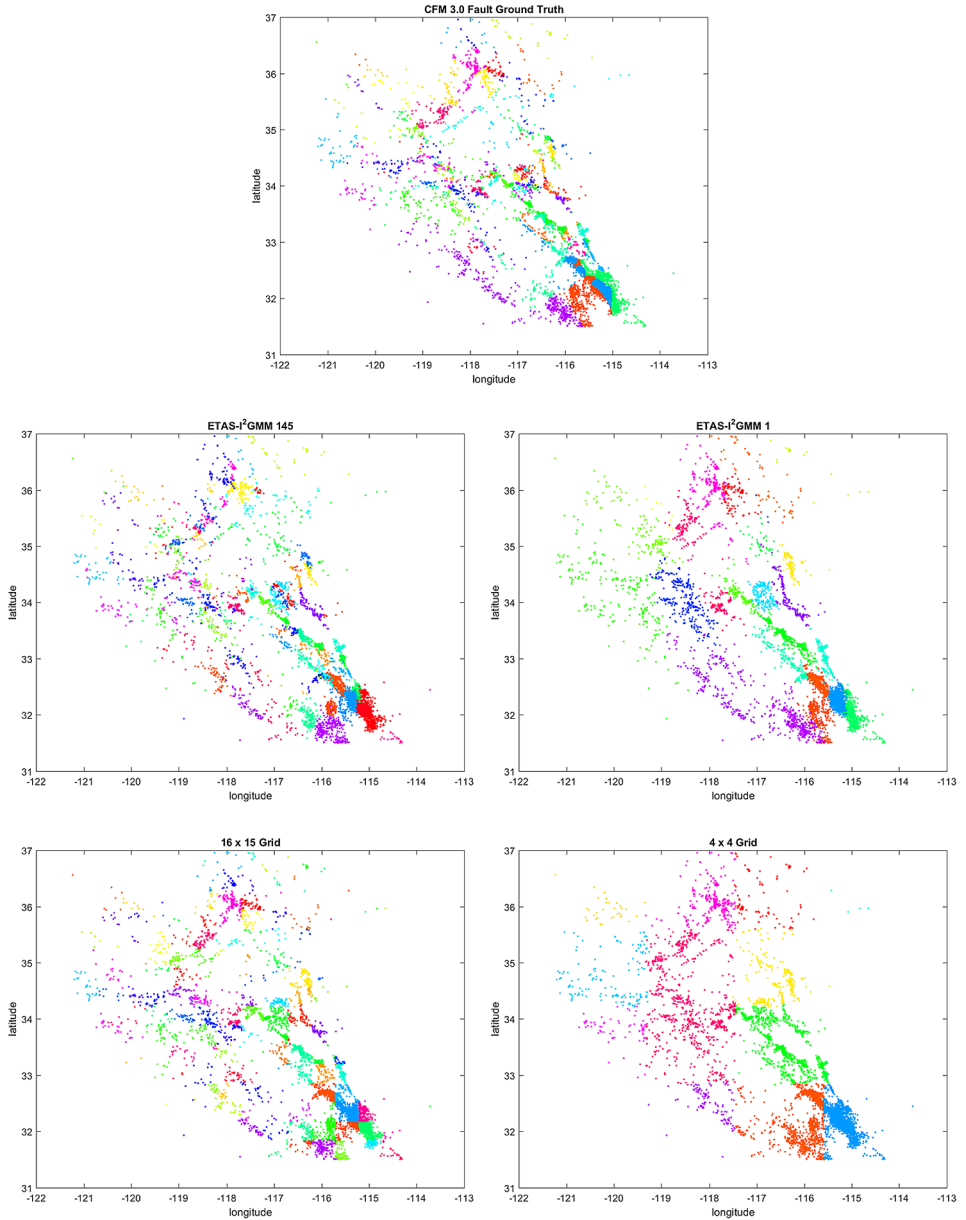
FIG. 4.   *True and predicted CFM fault groupings. Events with same labels are shown by the same color.*

4. Discussion.   We introduced a coupled ETAS-I^2GMM model for jointly estimating multi-scale clustering in earthquake data with parameters governing earthquake productivity and self-excitation. We also introduced what we believe is a
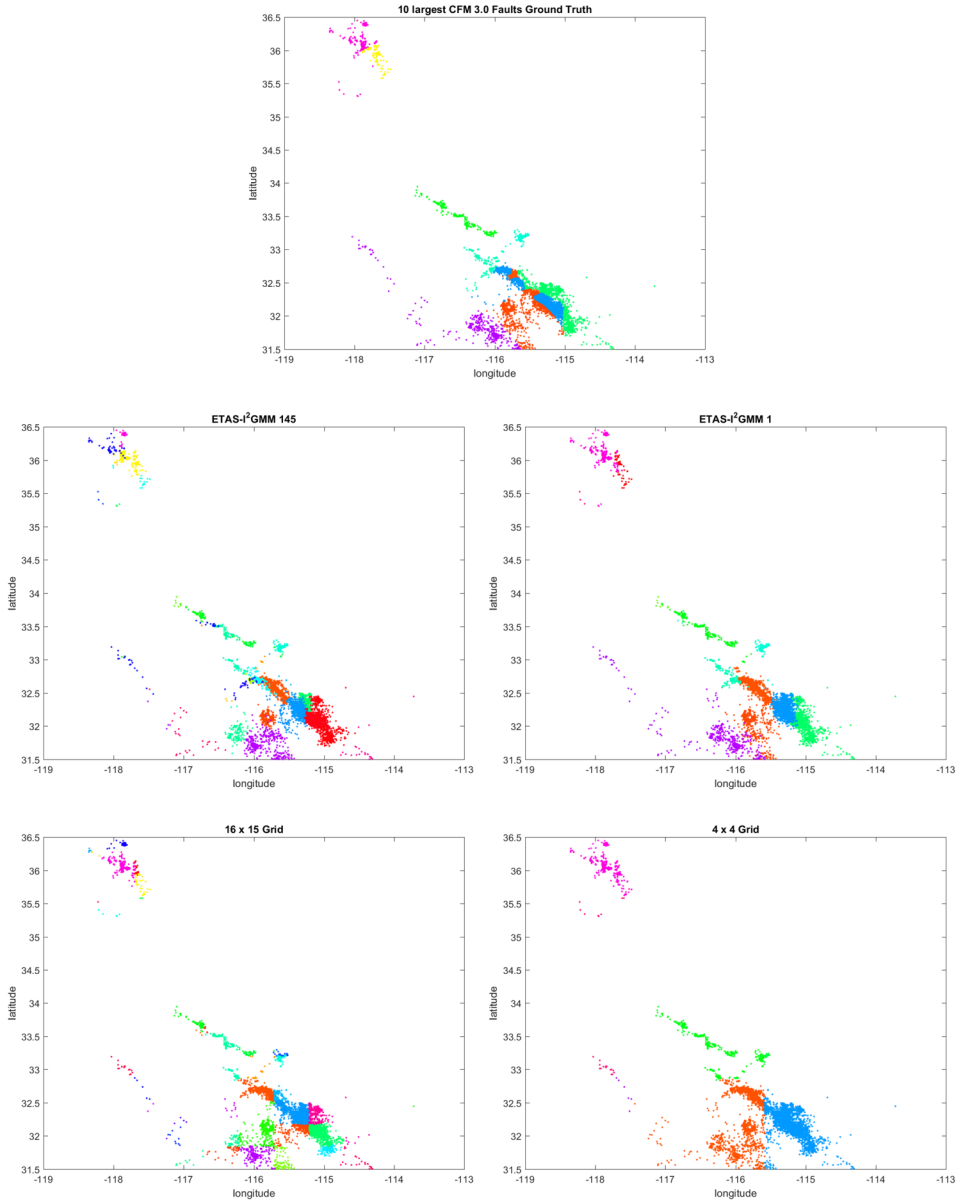
FIG. 5. 10 *largest CFM faults and recovered clusters. Events with same labels are shown by the same color.*

novel machine-learning task for statistical seismology, namely estimating CFM fault clusters using unlabeled space–time-magnitude event data. Improving upon algorithms aimed at solving this task could aid in the development of future versions of CFM, as well as fault models in other regions of the world.

The I²GMM model may have applications to point processes beyond those arising in seismology. Space–time self-exciting point processes arise in the study of crime [Mohler et al. (2011, 2015), Mohler (2014)], conflict [Lewis and Mohler (2011)], and terrorism [Mohler (2013), Porter and White (2012), White and Porter (2014), White, Porter and Mazerolle (2013)], as well as in social-network event dynamics, for example in social media [Lai et al. (2014), Simma and Jordan (2012), Zhao et al. (2015)]. In the case of crime, clusters arise naturally from the superposition of events committed by different offenders with different modi operandi. Similar clusters may arise from the operations of different terrorist groups within a geographic region. I²GMM is a flexible model for capturing this type of clustering in the intensity of events of a point process.

REFERENCES

ADELFIO, G. and CHIODI, M. (2015). Alternated estimation in semi-parametric space–time branching-type point processes with application to seismic catalogs. *Stoch. Environ. Res. Risk Assess.* **29** 443–450.

ANDREWS, J. L. and MCNICHOLAS, P. D. (2012). Model-based clustering, classification, and discriminant analysis via mixtures of multivariate *t*-distributions: The *t*EIGEN family. *Stat. Comput.* **22** 1021–1029. MR2950082

ARCHAMBEAU, C. and VERLEYSEN, M. (2007). Robust Bayesian clustering. *Neural Netw.* **20** 129–138.

BAUDRY, J.-P., RAFTERY, A. E., CELEUX, G., LO, K. and GOTTARDO, R. (2010). Combining mixture components for clustering. *J. Comput. Graph. Statist.* **19** 332–353. MR2758307

FERGUSON, T. S. (1973). A Bayesian analysis of some nonparametric problems. *Ann. Statist.* **1** 209–230. MR0350949

FIGUEIREDO, M. A. and JAIN, A. K. (2002). Unsupervised learning of finite mixture models. *IEEE Trans. Pattern Anal. Mach. Intell.* **24** 381–396.

FORBES, F. and WRAITH, D. (2014). A new family of multivariate heavy-tailed distributions with variable marginal amounts of tailweight: Application to robust clustering. *Stat. Comput.* **24** 971–984. MR3253848

GARDNER, J. K. and KNOPOFF, L. (1974). Is the sequence of earthquakes in Southern California, with aftershocks removed, Poissonian? *Bull. Seismol. Soc. Am.* **64** 1363–1367.

GE, Y. and SEALFON, S. C. (2012). FlowPeaks: A fast unsupervised clustering for flow cytometry data via K-means and density peak finding. *Bioinformatics* **28** 2052–2058.

HENNIG, C. (2010). Methods for merging Gaussian mixture components. *Adv. Data Anal. Classif.* **4** 3–34. MR2639661

KUHN, H. W. (1955). The Hungarian method for the assignment problem. *Nav. Res. Logist. Q.* **2** 83–97. MR0075510

LAI, E., MOYER, D., YUAN, B., FOX, E., HUNTER, B., BERTOZZI, A. L. and BRANTINGHAM, J. (2014). Topic time series analysis of microblogs. Technical report, DTIC Document.

LEE, S. and MCLACHLAN, G. J. (2014). Finite mixtures of multivariate skew *t*-distributions: Some recent and new results. *Stat. Comput.* **24** 181–202. MR3165547

LEWIS, E. and MOHLER, G. (2011). A nonparametric EM algorithm for multiscale Hawkes processes. Preprint available at http://paleo.sscnet.ucla.edu/Lewis-Molher-EM_Preprint.pdf.

MARSAN, D. and LENGLINE, O. (2008). Extending earthquakes' reach through cascading. *Science* **319** 1076–1079.

MOHLER, G. (2013). Modeling and estimation of multi-source clustering in crime and security data. *Ann. Appl. Stat.* **7** 1525–1539. MR3127957

MOHLER, G. (2014). Marked point process hotspot maps for homicide and gun crime prediction in Chicago. *Int. J. Forecast.* **30** 491–497.

MOHLER, G. O., SHORT, M. B., BRANTINGHAM, P. J., SCHOENBERG, F. P. and TITA, G. E. (2011). Self-exciting point process modeling of crime. *J. Amer. Statist. Assoc.* **106** 100–108. MR2816705

MOHLER, G. O., SHORT, M. B., MALINOWSKI, S., JOHNSON, M., TITA, G. E., BERTOZZI, A. L. and BRANTINGHAM, P. J. (2015). Randomized controlled field trials of predictive policing. *J. Amer. Statist. Assoc.* **110** 1399–1411. MR3449035

OGATA, Y. (1988). Statistical models for earthquake occurrences and residual analysis for point processes. *J. Amer. Statist. Assoc.* **83** 9–27.

OGATA, Y. (1998). Space–time point-process models for earthquake occurrences. *Ann. Inst. Statist. Math.* **50** 379–402.

PEEL, D. and McLACHLAN, G. J. (2000). Robust mixture modelling using the t distribution. *Stat. Comput.* **10** 339–348.

PLESCH, A., SHAW, J. H., BENSON, C., BRYANT, W. A., CARENA, S., COOKE, M., DOLAN, J., FUIS, G., GATH, E. and GRANT, L. (2007). Community fault model (CFM) for southern California. *Bull. Seismol. Soc. Am.* **97** 1793–1802.

PORTER, M. D. and WHITE, G. (2012). Self-exciting hurdle models for terrorist activity. *Ann. Appl. Stat.* **6** 106–124. MR2951531

SCEDC (2013). Southern California earthquake center. https://service.scedc.caltech.edu/eq-catalogs/. Caltech.Dataset. DOI:10.7909/C3WD3xH1.

SIMMA, A. and JORDAN, M. I. (2012). Modeling events with cascades of Poisson processes. Preprint ArXiv:1203.3516.

SPENCE, W., SIPKIN, S. A. and CHOY, G. L. (1989). Measuring the size of an earthquake. *Earthquake Information Bulletin* (*USGS*) **21** 58–63.

STEPHENS, M. (2000). Dealing with label switching in mixture models. *J. R. Stat. Soc. Ser. B. Stat. Methodol.* **62** 795–809. MR1796293

SUN, J., KABAN, A. and GARIBALDI, J. M. (2010). Robust mixture modeling using the Pearson type VII distribution. In *Neural Networks* (*IJCNN*), *the* 2010 *International Joint Conference on* 1–7. IEEE.

SVENSÉN, M. and BISHOP, C. M. (2005). Robust Bayesian mixture modelling. *Neurocomputing* **64** 235–252.

UTSU, T. (1961). A statistical study on the occurrence of aftershocks. *Geophys. Mag.* **30** 521–605.

VEEN, A. and SCHOENBERG, F. P. (2008). Estimation of space–time branching process models in seismology using an EM-type algorithm. *J. Amer. Statist. Assoc.* **103** 614–624. MR2523998

WHITE, G. and PORTER, M. D. (2014). GPU accelerated MCMC for modeling terrorist activity. *Comput. Statist. Data Anal.* **71** 643–651. MR3131995

WHITE, G., PORTER, M. D. and MAZEROLLE, L. (2013). Terrorism risk, resilience, and volatility: A comparison of terrorism in three Southeast Asian countries. *J. Quant. Criminol.* **29** 295–320.

YEREBAKAN, H. Z., RAJWA, B. and DUNDAR, M. (2014). The infinite mixture of infinite Gaussian mixtures. In *Advances in Neural Information Processing Systems* 28–36.

ZALIAPIN, I., GABRIELOV, A., KEILIS-BOROK, V. and WONG, H. (2008). Clustering analysis of seismicity and aftershock identification. *Phys. Rev. Lett.* **101** 018501.

ZHAO, Q., ERDOGDU, M. A., HE, H. Y., RAJARAMAN, A. and LESKOVEC, J. (2015). Seismic: A self-exciting point process model for predicting tweet popularity. In *Proceedings of the* 21*th ACM SIGKDD International Conference on Knowledge Discovery and Data Mining* 1513–1522. ACM.

Y. CHENG, M. DUNDAR AND G. MOHLER

ZHUANG, J. (2011). Next-day earthquake forecasts for the Japan region generated by the ETAS model. *Earth Planets Space* **63** 5.

ZHUANG, J., OGATA, Y. and VERE-JONES, D. (2002). Stochastic declustering of space–time earthquake occurrences. *J. Amer. Statist. Assoc*. **97** 369–380. MR1941459

COMPUTER & INFORMATION SCIENCE
INDIANA UNIVERSITY–PURDUE UNIVERSITY INDIANAPOLIS
INDIANAPOLIS, INDIANA 46202
USA
E-MAIL: chengyic@iupui.edu
        mdundar@iupui.edu
        gmohler@iupui.edu